

Article

The Effect of an External Electric Field on the Electronic Properties of Defective CBN Nanotubes: A Density Functional Theory Approach

Saed Salman ^{1,*}, Najeh Rekik ², Alaaedeen Abuzir ¹, Adil Alshoaibi ¹ and Jamal Suleiman ¹

¹ Department of Physics, College of Science, King Faisal University, P.O. Box 400, Al-Ahsa 31982, Saudi Arabia; aabuzir@kfu.edu.sa (A.A.); adshoaibi@kfu.edu.sa (A.A.); jsuleiman@kfu.edu.sa (J.S.)

² Department of Chemistry, University of Alberta, Edmonton, AB T6G 2G2, Canada; rekik@ualberta.ca

* Correspondence: ssalman@kfu.edu.sa

Abstract: We investigated the effects of applying an external electric field on the electronic properties of Stone-Wales (SW) defective carbon-boron-nitride nanotubes (CBN) using first principles calculations. The defective CBN nanotubes were modeled by introducing Stone-Wales defects in the boron-nitride segment (BN-SW), the carbon segment (C-SW), and the carbon-boron-nitride interface segment (CBN-SW). Initially, we studied the formation energies and the structural stability for all models. As a result of adding the SW defects, the calculated bandgap values of the C-SW and CBN-SW models showed significant changes compared to the pristine CBN nanotube. Meanwhile, the BN-SW model showed a slight bandgap change because of the strong covalent bonding between the boron and nitrogen atoms. Applying a transverse electric field induced a fast bandgap closing response in all models, indicating a rapid semiconductor-to-metal phase transition. The defective C-SW and CBN-SW models demonstrated unique bandgap closing patterns in response to applied transverse and longitudinal electric fields, while pristine and BN-SW models had similar bandgap responses.

Keywords: electronic properties; heterostructured CBN nanotubes; external electric field; Stone-Wales defects; density functional theory



Citation: Salman, S.; Rekik, N.; Abuzir, A.; Alshoaibi, A.; Suleiman, J. The Effect of an External Electric Field on the Electronic Properties of Defective CBN Nanotubes: A Density Functional Theory Approach. *Crystals* **2022**, *12*, 321. <https://doi.org/10.3390/cryst12030321>

Academic Editor: Rajratan Basu

Received: 13 January 2022

Accepted: 22 February 2022

Published: 25 February 2022

Publisher's Note: MDPI stays neutral with regard to jurisdictional claims in published maps and institutional affiliations.



Copyright: © 2022 by the authors. Licensee MDPI, Basel, Switzerland. This article is an open access article distributed under the terms and conditions of the Creative Commons Attribution (CC BY) license (<https://creativecommons.org/licenses/by/4.0/>).

1. Introduction

Directly after carbon nanotubes were discovered by Iijima in 1991 [1], intensive theoretical and experimental studies were sparked to investigate the different properties of nanotubes. In particular, the exceptional electrical, mechanical, and optical properties of nanotube materials attracted the interests of many scientists [2–4]. Due to their promising applications, different one-dimensional nanotube structures (chiralities) were proposed based on rolling up a single hexagonal monolayer of different materials. After carbon nanotubes (CNTs) and boron-nitride nanotubes (BNNTs) were synthesized, other nanotube structures such as aluminum-nitride nanotubes (ALNNTs) and silicon-carbide nanotubes (SICNTs) were predicted [5–8]. A broad range of tunable properties was achieved by assembling different segments of conventional nanotubes. Thus, hexagonal layers of different atomic segments were rolled up to form heterostructure nanotubes to achieve certain physical properties. The newly formed heteronanotubes appeared to be promising candidates for developing practical and efficient nanodevices. Heteronanotubes were theoretically developed and studied, and advancements in nanomaterial synthesis provided an opportunity to study various unknown properties of synthesized heteronanotubes. CNTs depend on their chirality for their electronic properties, while BNNTs are considered wide energy gap semiconductors, and their electronic properties are independent of the tube chirality. Therefore, BNNT is one of the most interesting non-carbon nanotubes. Since BN nanotubes and carbon nanotubes have similar lattice structures, CBN heterostructured nanotubes were proposed. One CBN heterostructured nanotube has attracted the interest of

several research groups because its carbon atoms form bonds with both nitrogen and boron atoms [4–6,9]. Bonding between atoms with different numbers of valence electrons can change the electronic properties of its two combined hexagonal structures; it is therefore unique and promising for the achievement of properties that were not present in two other pristine nanotubes. In addition, the electronic properties of CNT and BNNT heterostructures can be tuned by altering their atomic structure and configuration. The electronic properties of CBN heteronanotubes have been theoretically investigated for zigzag and armchair heteronanotubes [10]. The combination of two carbon and boron nitride cylindrical segments in a nanotube structure can create a built-in static electric field along the tube axis [11]. Furthermore, the transport properties of different-chirality CBN heteronanotubes have been investigated using non-equilibrium Green's function techniques and density functional theory [12]. The thermal resistance of carbon-boron-nitride heterostructures has also been studied by molecular dynamics simulations [13]. In contrast, CBN heteronanotubes have been synthesized by chemical vapor deposition at elevated temperatures, and their electronic properties were primarily determined by their composition, which can be easily controlled [14]. Additionally, different growth schemes of CBN nanotubes have been achieved by laser ablation [6]. Finally, C and BN nanotube layers have been synthesized separately by an arc-discharge technique [15]. During synthesis, accidental Stone-Wales (SW) defects take place, which are an expected structural imperfection in graphene-like materials [16]. Defects of this type have been shown to have crucial roles in modifying the electronic properties of nanotubes and their hexagonal layer derivatives. Stone-Wales defect formation involves the rotation of the two bonded atoms by 90° around their middle point [17]. Consequently, the four head-to-head hexagons transform into two heptagons and two pentagons (7-5 pairs). Stone-Wales Defects of the (7-5) type have been intentionally produced in the laboratory [10]. Stone-Wales defects have improved the adsorption ability of different types of atoms in carbon nanotubes. Using density functional calculations, applying transverse and longitudinal electric fields on silicon-carbide nanotubes (SiCNTs) with differently orientated Stone-Wales defects results in a significant decrease in bandgap energy [18]. In another work, Stone-Wales defects were found to reduce the bandgap of carbon boron nitride heterostructured nanotubes [19]. Applying external electric fields to different nanostructures has provided a practical approach for the design and tuning of carbon and boron-nitride-based nanostructures in a wide variety of nano electronic applications, including sensing devices, switches, and static memory cells [20–22]. It has been reported that applying an external electric field can achieve high control and the precise selectivity of CO_2 molecules on hexagonal boron-nitride nanosheets [20]. Moreover, applying a longitudinal external electric field modulates the sensing ability of single-walled carbon and carbon nitride nanotubes to detect aspirin molecules [21]. On the other hand, it has also been found that the fast semiconductor-to-metal response of one-dimensional and two-dimensional nanostructures to applied external electric fields can overcome the technical switching challenges in memory device technologies [22]. Finally, in this work, the band gap responses of a pristine and a defective heterostructured CBN in response to applied external electric fields can provide clues for identifying defective structures and defect types [18].

In this work, we modeled three defective CBN nanotubes by introducing an individual Stone-Wales defect at various locations on the CBN pristine nanotubes. We performed density functional theory calculations for every modeled structure to study the formation energies, the structural stability, and the electrical effects of different types of Stone-Wales defects on the zigzag (9,0) CBN heterostructure nanotubes. We also studied the effects of longitudinal and transverse electric fields on the nanotubes' electronic properties. We carried out a unique and in-depth study and we compared our results to pure and defective carbon, boron-nitride, and silicon-carbide. To the best of the authors' knowledge, this study has not been previously performed.

2. Computational Details

Density functional calculations were used to perform the electronic structure calculations, using “Cambridge Serial Total Energy Package” (CASTEP) code. A supercell was used to build the simulated structures with the lattice constants a , b , and c . To avoid interactions between two adjacent tube images, the lattice constants a and b were set to be 25 \AA [23]. To maintain the tube periodicity in the axial direction, the length of the lattice constant “ c ” was initially set equal to the nanotube axial lattice constant. To minimize the total electronic energy and to relax the nanotubes, we performed geometry optimization using generalized gradient approximation (GGA) for the exchange-correlation functional with revised Perdew-Burke-Ernzerh (RPBE) parameterization. Initially, without applying the external fields, all under study structures were optimized to a point where the maximum applied force on each atom was less than 0.02 eV/\AA^{-1} [24]. In addition, the maximum displacement of atoms, the self-consistent field (SCF) tolerance, and the maximum stress value were set to be 0.001 \AA , $1 \times 10^{-5} \text{ eV/atom}$, and 0.04 GPa , respectively. The Monkhorst-Pack mesh of $(1 \times 1 \times 8)$ K-points was utilized to sample the one-dimensional Brillion zone, which was calculated after rigorous testing [25]. while the plane wave cutoff energy point was fixed at 500 eV . Finally, external uniform electric fields were applied in the range of 0.0 to 1.5 eV/\AA/e .

3. Results and Discussion

3.1. Stability and Band Structure

In this study, we used longitudinal and transverse electric fields to tune the electronic properties of Stone-Wales defective CBN nanotubes. We used four models of zigzag $(9,0)$ $\text{C}_{0.5}(\text{BN})_{0.5}$ nanotubes to perform our calculations (Figure 1).

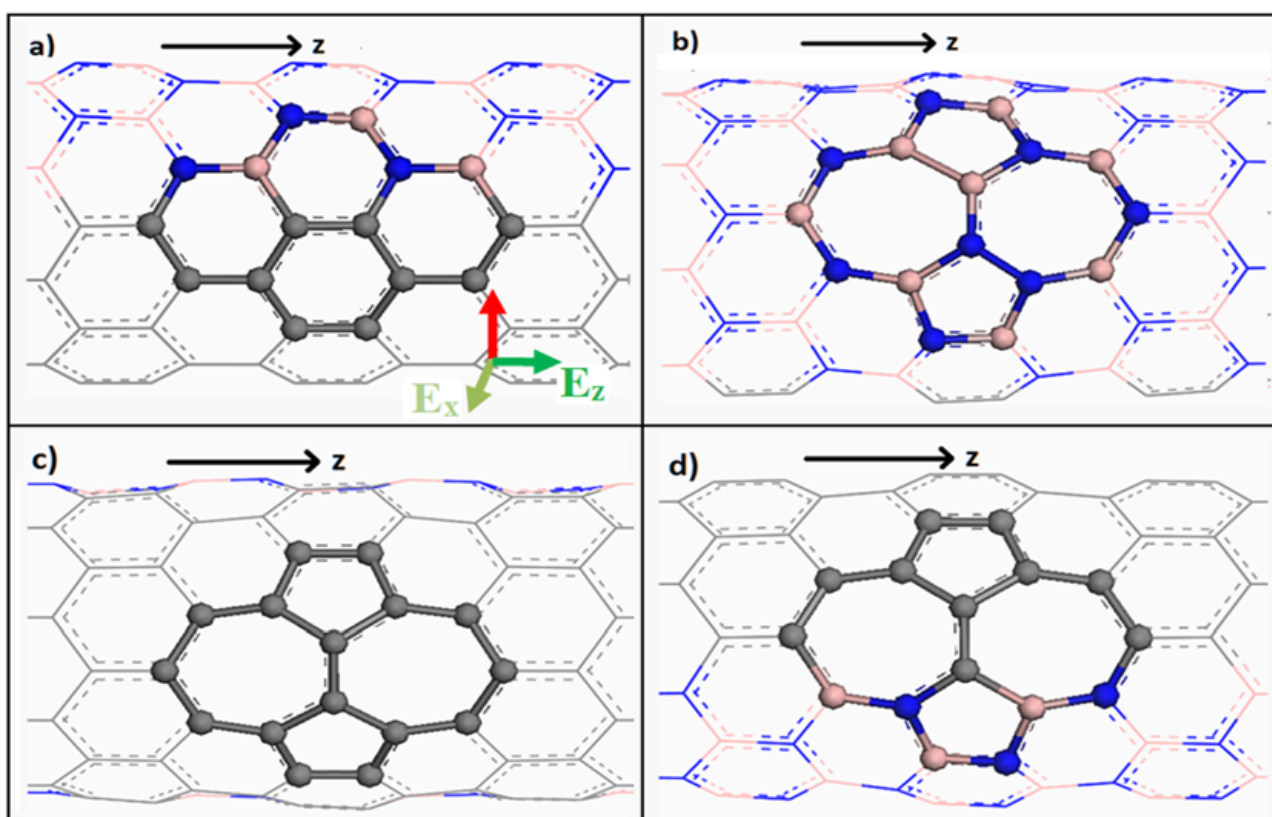


Figure 1. Stone-Wales defective models; (a) Pristine CBN nanotube, (b) Boron nitride CBN model (BN-SW), (c) Carbon CBN model (C-SW), (d) Carbon and boron-nitride CBN model (CBN-SW); E_z denotes the longitudinal electric field in the axial direction, E_x denotes the transverse electric field in the radial direction.

The interface of the carbon-boron-nitride segments of the CBN nanotube was parallel to the z-axis of the tube (Figure 1a). In order to compare and simulate actual Stone-Wales defects that may occur randomly in CBN nanotubes, we modeled both the pristine nanotubule and the various types of Stone-Wales defects. The defective CBN nanotubes were modeled by introducing Stone-Wales defects in the boron-nitride (BN-SW) segment (Figure 1b), the carbon (C-SW) segment (Figure 1c), and finally, at the boundary of the carbon and boron-nitride (CBN-SW) segments (Figure 1d).

Initially, we calculated the formation energy (E_R) for the CBN nanotubes, which is the energy required for the formation of Stone-Wales defects on the nanotube surface. The formation energy (E_R) of a CBN nanotube is given by the following equation:

$$E_R = E_{SW} - E_{Pure} \quad (1)$$

where E_{Pure} and E_{SW} denote the total electronic energies of defect-free (E_{Pure}) and Stone-Wales-defected CBN (E_{SW}) nanotubes [26]. It is worth mentioning that, when Stone-Wales defects were introduced onto the CBN heterostructure models, the total number of carbon, boron, and nitrogen atoms remained the same as in the pristine CBN nanotube. Hence, there was no change in atomic number count. Therefore, the total electronic energy calculations were only affected by the newly formed Stone-Wales defects, which are formed by the rotation of the two bonded atoms by 90° around their middle point [17]. In order to gain a better understanding, the calculated total electronic and formation energies of SW defects of CBN nanotube systems are listed in Table 1.

Table 1. The total energy and the formation energy for all CBN nanotube models.

CBN Nanotube	Total Energy (eV)	Formation Energy (eV)
Pure	−17,827.77	—
C-SW	−17,824.64	3.13
B-SW	−17,823.32	4.45
CB-SW	−17,822.89	5.15

The formation energies of the defected C-SW, BN-SW, and CBN-SW heterostructure systems were 3.13 eV, 4.45 eV, and 5.12 eV, respectively. However, the pristine CBN structure had the minimum total electronic energy, which corresponds to the highest stability. As a consequence of SW defects in CBN nanotube heterostructures, the bonds rearrange so that the total electronic energy of the structure increases. The formation energy of the C-SW defect, located at the graphene segment of the tube, was evidently much lower than that of the CB-SW and BN-SW defects. This suggests that the highest stability is more likely when the defect appears at the graphene segment of the tube. Additionally, CB-SW defects at the CBN axial interface have a higher formation energy than BN-SW defects. This could be ascribed to the undesired redistribution of charges caused by the SW defect at the CBN interface segments. According to previous studies, the stability and electronic properties of CBN nanotube heterostructures are influenced by the structure of the interface [27,28]. It is also worth noting that C–C bonds have a significantly lower formation energy than B–N bonds, so a Stone-Wales defect in the B–N segment of the CBN tube is extremely unlikely [29]. On the other hand, the reported high rolling-up strain values in pristine boron-nitride nanotubes could also result in a higher formation energy in BN-SW defective CBN nanotubes [23].

Due to their ionic bonding properties, BNNTs show a stable and wide bandgap value of 5.5 eV, which was independent of the tube chirality and nearby tube-to-tube interactions, whereas the zigzag (9,0) CNT-which comprises the carbon segment-has a very small bandgap and is considered semi-metallic [4]. Graphene and boron-nitride segments are both bonded along the axial interface direction to form zigzag (9,0) $C_{0.5}(BN)_{0.5}$ nanotubes. Additionally, the minimal mismatch between the bond lengths of CNTs and BNNTs promotes the formation of zigzag (9,0) $C_{0.5}(BN)_{0.5}$ heterostructure nanotubes.

The Stone-Wales heptagon structures formed at the interface between the carbon and boron-nitride segments exhibit a significant increase in the length of C–B and C–N bonds [19]. Before applying any external fields, the bandgap of the pristine CBN nanotube was 0.784 eV, whereas when SW defects were incorporated, the bandgap changed to 0.462 eV, 0.788 eV, and 0.534 eV for C-SW, B-SW and CB-SW CBN heterostructures, respectively (Figure 2).

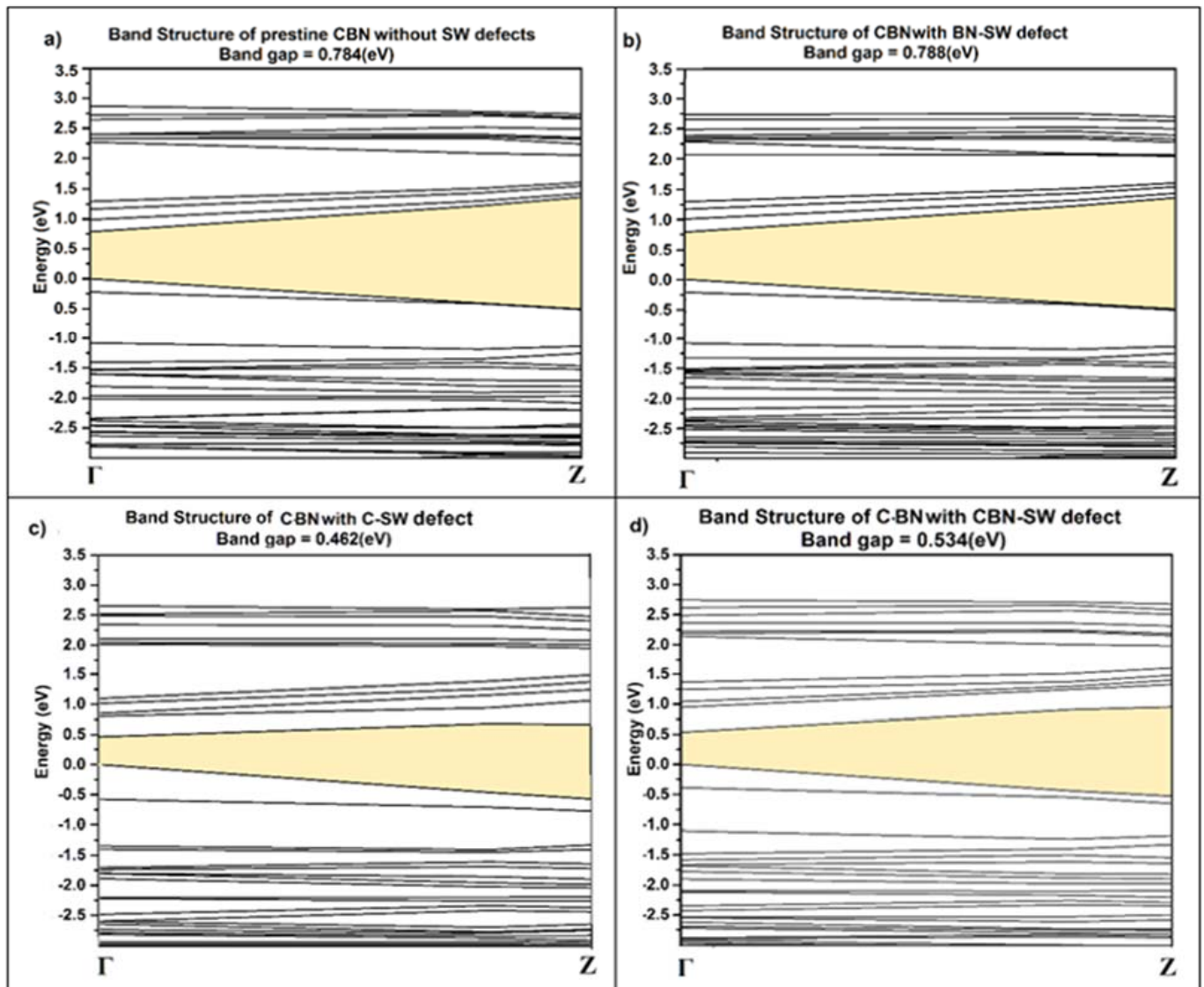


Figure 2. The band structure of for CBN models at zero applied electric field (a) Pristine CBN nanotube, (b) Boron nitride CBN model (BN-SW), (c) Carbon CBN model (C-SW), (d) Carbon and boron-nitride CBN model (CBN-SW).

Hence, Stone-Wales defects formed in C-SW and CB-SW structures showed significant differences in bandgap values compared to pristine CBN nanotubes. However, the greatest effect of Stone-Wales defects was noticed in the bandgap of the C-SW type, where Stone Wales defects appear at the carbon segment (Figure 2c). This may be attributed to the bond length variations between carbon atoms that affect the dispersion K point positions [4]. Likewise, the reduction in the bandgap of the defected CBN-SW structure could be explained by the contributed conductance enhancement by the affected C–N atoms at the C–B segment interfaces. Recent reports on radially coupled CBN heterostructures with Stone-Wales defects are consistent with this finding [30]. On the other hand, introducing SW defects into the B–N segment did not affect the bandgap value due to the robust covalent

bonding of the hexagonal BN structure. It is evident that the bandgap tuning sensitivity depends on the location of SW defects in BNC heterostructured nanotubes [31].

3.2. Longitudinal and Transverse Electric Field Effects

The CBN nanotube is characterized by a spontaneous and polarized electric field, which results from the interface between the polar B–N segment and the nonpolar carbon segment [11]. As both B and N atoms are one electron short and one electron rich in comparison to C, the polarization field has a profound effect on the total electrostatic potential of the CBN heterostructured nanotube. Considering the existence of the spontaneous polarization field, we introduced an external electric field to investigate the electronic properties of SW defected CBN heterostructured nanotubes. For both the longitudinal and transverse electric field, the constant electric field values were chosen from zero $\text{eV}/\text{\AA}/\text{e}$ and gradually increased to their maximum values, at which the bandgap closed and the semiconductor-to-metal transition occurred. Therefore, the minimum applied electric field value was set to zero and the maximum value was determined by the transition to the metallic state of the CBN nanotube models. Therefore, we monitored the bandgap variations while applying steady longitudinal electric fields (E_z) from $0.0 \text{ eV}/\text{\AA}/\text{e}$ to $1.5 \text{ eV}/\text{\AA}/\text{e}$ and transverse (E_x) electric fields from $0.0 \text{ eV}/\text{\AA}/\text{e}$ to $1.05 \text{ eV}/\text{\AA}/\text{e}$.

In order to handle the periodicity issue of the applied external electric field, an electric potential was added to the unit cell in the Hamiltonian. Hence, the effect of a homogeneous electric field across the tube region was modeled by a saw-tooth electric potential, i.e.,

$$V_{\text{ext}}(Z) = Ez \quad (-L/2 < Z < L/2) \quad (2)$$

where E is the value of the applied external electric field, while L is the length of the superlattice—which is chosen to be large enough so that the tube is located at the center of the superlattice, thus eliminating discontinuities at the boundary [32–35].

Additionally, to avoid unintended structural periodicity perturbations caused by the applied electric field, we allowed the system to relax after each screening step of the external field. Thus, the resulting superlattice expansion was considered and showed negligible structural deformation effects. Furthermore, the insignificant expansion of the superlattice parameters indicated nondestructive polarization and ionization effects.

The effects of the longitudinal electric field on the bandgap of CBN heterostructures are shown in Figure 3 and Table 2.

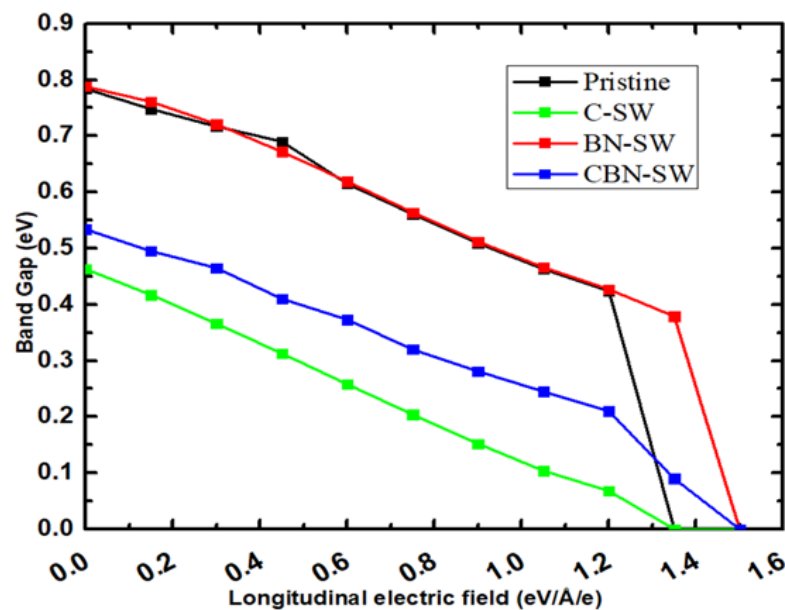


Figure 3. The band gap energies for pristine and Stone-Wales defected CBN models when an external longitudinal electric field is applied (The axial E_z -direction).

Table 2. The band gap values for the applied transverse electric field for all CBN nanotube models.

Transverse Electric Field (eV/Å/e)	Pure Type	C-SW Type	BN-SW Type	CBN-SW Type
0.00	0.784	0.463	0.788	0.534
0.15	0.785	0.473	0.789	0.507
0.30	0.781	0.479	0.783	0.465
0.45	0.772	0.479	0.757	0.411
0.60	0.733	0.462	0.434	0.352
0.75	0.509	0.255	0.048	0.063
0.90	0.051	0.051	0.007	0.000
1.05	0.000	0.000	0.000	0.000

Figure 3 shows that the bandgap narrows as the longitudinal electric field increases. As the semiconductor-to-metal phase transition occurs in CBN heterostructured nanotubes, the bandgaps decreased with increasing longitudinal electric field values (Figure 3). The bandgap decrease may be explained by the asymmetry of the electrostatic potential induced by the applied longitudinal electric field, where the bandgap is defined as the difference between the highest occupied molecular orbital (HOMO) and the lowest unoccupied molecular orbital (LUMO). Alternatively, higher electric fields are needed to combine adjacent sub-bands and substantially modify the band structure, which can lead to unexpected structural deformations—particularly if the nanotube has defects, like in SW defects. Furthermore, when a strong electric field is applied to a periodic nanotube, the aperiodic effect of the applied field cannot be overlooked. As the applied longitudinal electric field increases, the bandgap decreases almost linearly. On the other hand, the effect of the transverse electric field on the bandgap for CBN heterostructures is shown in Figure 4 and Table 3.

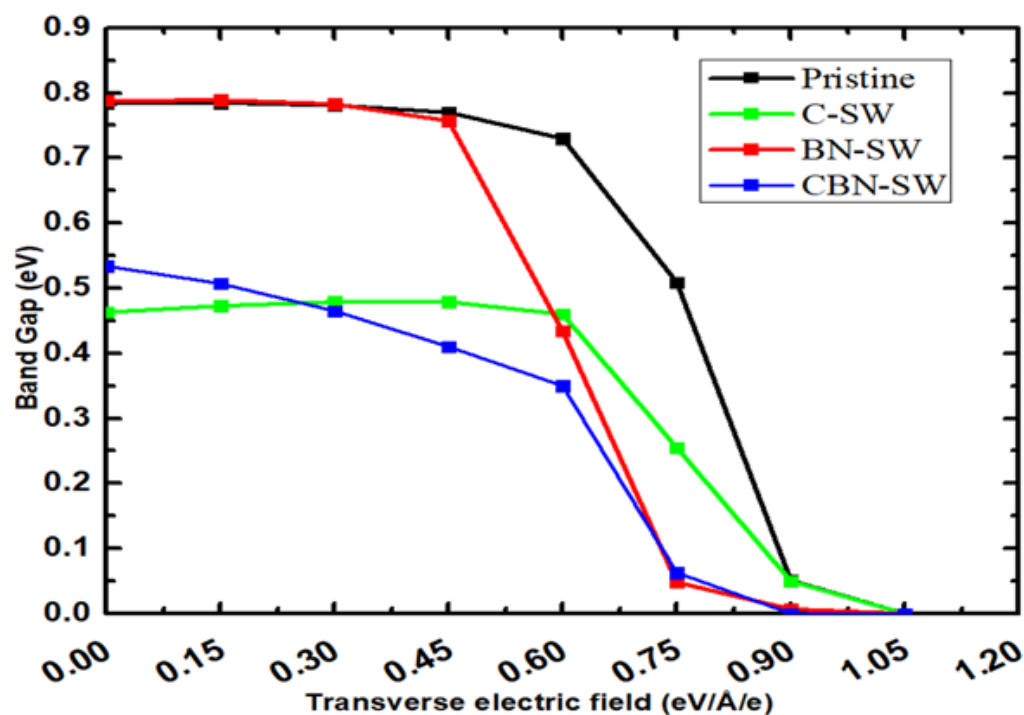
**Figure 4.** The band gap energies for pristine and Stone-Wales defected CBN models when an external transverse electric field is applied (The radial Ex-direction).

Table 3. Bandgap values for the applied longitudinal electric field for all the CBN nanotube models.

Longitudinal Electric Field (eV/Å/e)	Pure Type	C-SW Type	BN-SW Type	CBN-SW Type
0.00	0.784	0.463	0.788	0.534
0.15	0.748	0.417	0.761	0.495
0.30	0.717	0.366	0.721	0.465
0.45	0.691	0.313	0.672	0.410
0.60	0.615	0.258	0.619	0.373
0.75	0.561	0.204	0.564	0.320
0.90	0.509	0.152	0.512	0.281
1.05	0.463	0.104	0.466	0.245
1.20	0.424	0.068	0.427	0.210
1.35	0.000	0.000	0.379	0.091
1.50	0.000	0.000	0.000	0.000

As the external transverse electric field increased, the bandgaps quadratically decreased, as shown in Figure 4. This could be attributed to the induced localized separation of charges caused by the transverse electric field. While the top of the valence band charges moved in the same direction as the exerted electric field, the bottom of the conduction band charges moved in the opposite direction. Due to the built-up charge in regions of higher electric potential, the minimum value of the conduction band shifted down. Meanwhile, the maximum of the valence band shifted up due to the built-up charge in regions of low electric potential. In the non-degenerate valence and bottom conduction band states, the relationship between the small applied electric field and the bandgap is quadratic, according to the Stark effect. However, as the applied electric field increased, the electric potentials across the valence and conduction bands increased, resulting in a significant merging of the states of the two bands. Therefore, the bottom states of the conduction band (LOMO) and the top states of the valence band (HOMO) were modulated by the external electric field. The induced charges at the top of the valence band (HOMO) drifted towards the applied electric field and accumulated on one side of the BNC heterostructured nanotube, whereas the induced charges at the bottom of the conduction band (LOMO) drifted away from the applied electric field and accumulated on the other side to counteract the effects of the external electric field. Hence, the conduction band reduced its energy by accumulating the induced charges at high electric potential zones. In the meantime, the valence band buildup induced charges in low electric potential zones, narrowing the bandgap of the nanotube.

It is evident that when external longitudinal and transverse electric fields are applied, the bandgaps shrink—although the reduction trend is greater with the transverse electric field (Figures 3 and 4). In comparison to the longitudinal electric field, the fast semiconductor-metal phase transition observed in response to the applied transverse electric field can be explained by the shorter distance over which charges accumulated on one side of the BNC heterostructured nanotube. On the other hand, when the longitudinal electric field was applied in the Z-direction, the bandgap energy decreased quasi-linearly to zero. The effect on C-SW and CBN-SW Stone-Wales defects can be clearly seen when $E_z > 1.2 \text{ eV}/\text{Å}/e$ (refer to Figure 4). The linear response of the bandgap in the C-SW and CBN-SW Stone-Wales defected models could be attributed to the perturbation caused by Stone–Wales bond reorientation and reformation, which affects the conducting electrons in the carbon and boron-nitride segments of the CBN nanotube. On the other hand, the BN-SW and pristine nanotubes showed similar responses to the applied longitudinal electric field, which can be explained by the minor effects on the strong covalent bonds in the BN-SW defected segment. When compared to pure CBN nanotubes, the insignificant bandgap variations in BN-SW were in a good agreement with recently reported results for Stone–Wales defected BN nanosheets [36]. On the other hand, the response of the bandgap of the defected models to the transverse electric field was slightly different. We observed three interesting phenomena when we applied different values of transverse electric fields to pristine and Stone-Wales defected CBN nanotubes. To start with, regardless of whether

Stone-Wales defects were present or not, all samples underwent a semiconductor-metal phase transition. Compared to the applied longitudinal electric field, the pristine and Stone-Wales bandgap responses showed a faster semiconductor-metal phase transition response. Nonetheless, the initial steadily responses of the bandgap, however, were caused by the transverse electric field pointing in the opposite direction to the dipole moments located at the interface segments of the CBN nanotube. On the other hand, the bandgap value decreased gradually as the nearly-free electron band moved to one side of the unit cell as the transverse electric field was applied. As a result, applying a transverse electric field reallocated the edge-state densities evenly, causing the nearly-free electron band to quickly minimize and finally close. Finally, both the pristine and BN-SW models showed similar responses to the applied longitudinal electric field, which can be explained by the minor effect of the BN-SW defects on the strong B-N covalent bonds. It is interesting to note that both the pristine and BN-SW models showed similar responses to the applied transverse and longitudinal electric fields when compared to the C-SW and CBN-SW models. In contrast to the C-SW model, the insignificant variations in the bandgap values of the BN-SW model were caused by the strong covalent bonds between the boron and nitrogen atoms, which dominate the formation of BN-SW defects in the B-N segment. As a result, when transverse or longitudinal electric fields were applied, the BN-SW defected structure was the least affected, compared to the C-SW and CBN-SW models.

Finally, for both the pure and defected CBN models, the total density of states (TDOS) and the partial density of states (PDOS) were investigated (Figure 5). The separations of the partial density of states near the Fermi level resembled the calculated bandgap values from the band structure. The PDOS calculations showed that the observed peaks next to the Fermi level were mainly 2p electron orbitals, and no s electron orbitals were observed.

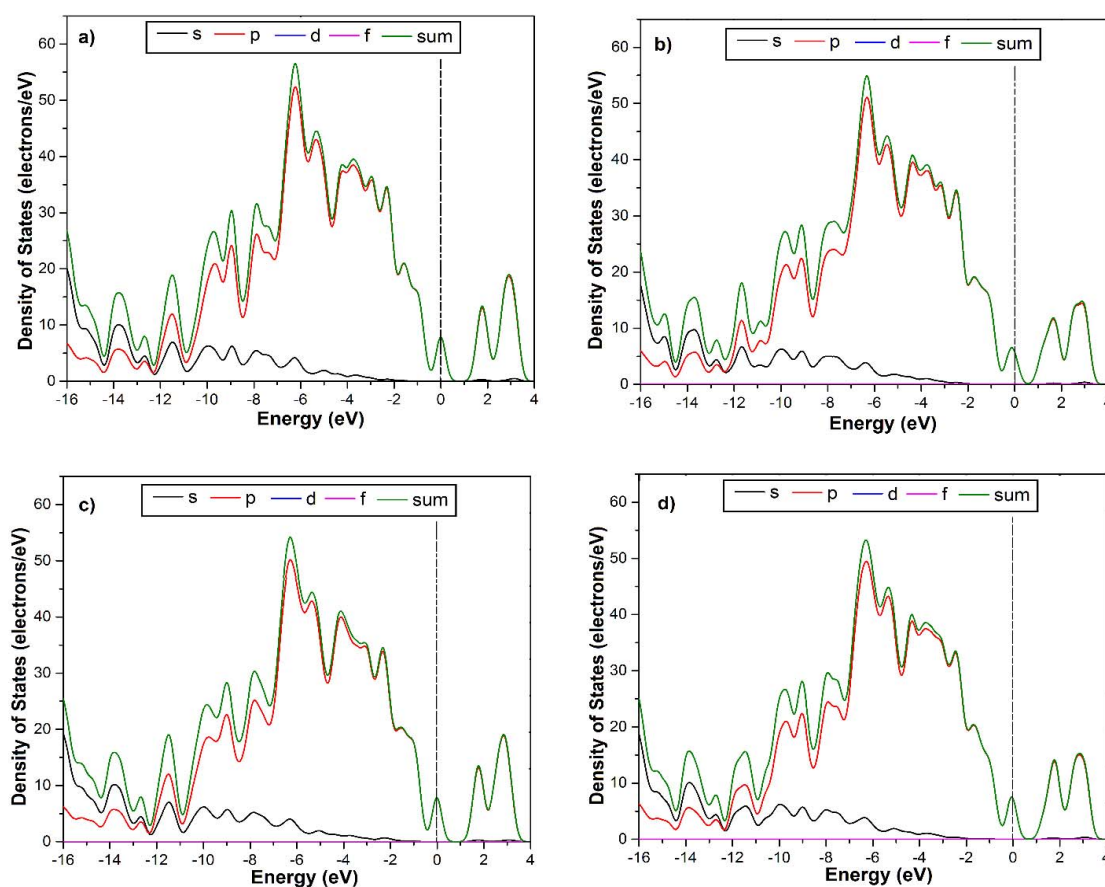


Figure 5. Total and partial density of states (PDOS and TDOS) for pristine and Stone-Wales defected CBN models with zero applied electric field: (a) Pristine CBN nanotube, (b) C-SW CBN model, (c) BN-SW CBN model, (d) CBN-SW CBN model. The vertical dashed line indicates the Fermi energy.

4. Conclusions

The effects of applying an external electric field on the electronic properties of Stone-Wales (SW) defective carbon-boron-nitride nanotubes (CBN) were studied by density functional theory. Initially, we calculated the electronic energies of the pristine and the defective CBN nanotubes and we found that the highest stability was more likely when the SW defect was located on the carbon segment. This can be attributed to the significantly lower formation energy of the C-C bonds when compared to B-N bonds, so that a Stone-Wales defect in the B-N segment of the CBN tube was extremely unlikely. At zero applied electric fields, the calculated bandgap values of the C-SW and CBN-SW models were significantly different from defect-free CBN nanotubes; however, the bandgap value of the BN-SW model was almost unaffected due to the strong covalent bonds between the boron and nitrogen atoms. As a result of applying longitudinal and transverse electric fields, all samples under study underwent a semiconductor-to-metal phase transition. The bandgap energy decreased quasi-linearly to zero in response to the applied longitudinal electric field. The longitudinal electric field had a noticeable effect on C-SW and CBN-SW models when $E_z > 1.2 \text{ eV/\AA/e}$, which could be attributed to the perturbation caused by Stone-Wales bond reorientation and reformation, which affects the conducting electrons in both the carbon and boron-nitride segments of the nanotube. When a transverse electric field was applied to all models, a fast bandgap closing response was observed, indicating a rapid semiconductor-to-metal phase transition. This might be explained by the shorter distance over which charges accumulated on one side of the BNC heterostructured nanotubes. The bandgap showed initial steady responses because the applied transverse electric field pointed in a direction opposite to the dipole moments located at the interface segments of the CBN nanotube. Then, the bandgap value decreased gradually over time as the nearly-free electron band moved to one side of the unit cell with the application of a transverse electric field. Finally, both the pristine and BN-SW models showed similar responses to the applied transverse and longitudinal electric fields when compared to the C-SW and CBN-SW models. The observed insignificant bandgap value variations of the defective BN-SW model in response to the applied electric fields can be attributed to the strong covalent bonds between the boron and nitrogen atoms, which dominate the structural formation of BN-SW defects in the B-N segment. With this work, we hope to shed some light on predicting SW defects and to be able to tune the electronic properties of pristine and defected CBN nanotubes with external electric fields for future nano-based electronic and optoelectronic applications.

Author Contributions: Conceptualization, S.S.; methodology, S.S., N.R.; software, S.S.; validation, N.R., A.A. (Alaaedeen Abuzir) and A.A. (Adil Alshoaibi); formal analysis, S.S.; investigation, S.S., N.R.; resources, N.R., J.S.; data curation, S.S.; writing—original draft preparation, S.S.; writing—review and editing, S.S., A.A. (Alaaedeen Abuzir) and A.A. (Adil Alshoaibi); visualization, J.S., N.R.; supervision, S.S.; project administration, S.S.; funding acquisition, S.S. All authors have read and agreed to the published version of the manuscript.

Funding: This research was funded by Deanship of Scientific Research at the King Faisal University grant number [1811026].

Data Availability Statement: Not applicable.

Acknowledgments: The authors acknowledge the Deanship of Scientific Research at the King Faisal University for their financial support under (Grant No. 1811026).

Conflicts of Interest: The authors declare no conflict of interest.

References

1. Iijima, S. Helical microtubules of graphitic carbon. *Nature* **1991**, *354*, 56–58. [[CrossRef](#)]
2. Chibotaru, L.F.; Compernelle, S.; Ceulemans, A. Electron transmission through atom-contacted carbon nanotubes. *Phys. Rev. B* **2003**, *68*, 125412–125443. [[CrossRef](#)]

3. Yu, S.S.; Wen, Q.B.; Zheng, W.; Jiang, Q. Effects of doping nitrogen atoms on the structure and electronic properties of zigzag single-walled carbon nanotubes through first-principles calculations. *Nanotechnology* **2007**, *18*, 165702. [[CrossRef](#)]
4. Salman, S.; Talla, J.; Abuzir, A.; Yasin, E. Uniaxial Strain Effects on Electronic Properties of Non-Armchair Single-Walled Carbon Nanotubes: First Principles Study. *J. Comput. Theor. Nanosci.* **2015**, *12*, 5265–5272. [[CrossRef](#)]
5. Wang, W.L.; Bai, X.D.; Liu, K.H.; Xu, Z.; Golberg, D.; Bando, Y.; Wang, E.G. Direct Synthesis of B–C–N Single-Walled Nanotubes by Bias-Assisted Hot Filament Chemical Vapor Deposition. *J. Am. Chem. Soc.* **2006**, *128*, 6530–6531. [[CrossRef](#)] [[PubMed](#)]
6. Zhang, Y.; Gu, H.; Suenaga, K.; Iijima, S. Heterogeneous growth of B-C-N nanotubes by laser ablation. *Chem. Phys. Lett.* **1997**, *279*, 264–269. [[CrossRef](#)]
7. Menon, M.; Richter, E.; Mavrandonakis, A.; Froudakis, G.; Andriotis, A.N. Structure and stability of SiC nanotubes. *Phys. Rev. B* **2004**, *69*, 115322. [[CrossRef](#)]
8. Noei, M.; Soleymanabadi, H.; Peyghan, A.A. Aluminum nitride nanotubes. *Chem. Pap.* **2016**, *71*, 881–893. [[CrossRef](#)]
9. Fathalizadeh, A.; Pham, T.; Mickelson, W.; Zettl, A. Scaled Synthesis of Boron Nitride Nanotubes, Nanoribbons, and Nanococoons Using Direct Feedstock Injection into an Extended-Pressure, Inductively-Coupled Thermal Plasma. *Nano Lett.* **2014**, *14*, 4881–4886. [[CrossRef](#)]
10. Du, A.; Chen, Y.; Zhu, Z.; Lu, G.; Smith, S. C-BN Single-Walled Nanotubes from Hybrid Connection of BN/C Nanoribbons: Prediction by ab initio Density Functional Calculations. *J. Am. Chem. Soc.* **2009**, *131*, 1682–1683. [[CrossRef](#)]
11. Beheshtian, J.; Sadeghi, A.; Neek-Amal, M.; Michel, K.H.; Peeters, F.M. Induced polarization and electronic properties of carbon-doped boron nitride nanoribbons. *Phys. Rev. B* **2012**, *86*, 195433. [[CrossRef](#)]
12. Wu, M.M.; Zhong, X.; Wang, Q.; Sun, Q.; Pandey, R.; Jena, P. Anisotropy and Transport Properties of Tubular C-BN Janus Nanostructures. *J. Phys. Chem. C* **2011**, *115*, 23978–23983. [[CrossRef](#)]
13. Xue, S.-W.; Chen, J.; Zhang, J. Self-Healing of Stone–Wales Defects in Boron Nitride Monolayer by Irradiation: Ab Initio Molecular Dynamics Simulations. *Chin. Phys. Lett.* **2013**, *30*, 103102. [[CrossRef](#)]
14. Yu, J.; Li, J.; Zhang, W.; Chang, H. Synthesis of high quality two-dimensional materials via chemical vapor deposition. *Chem. Sci.* **2015**, *6*, 6705–6716. [[CrossRef](#)]
15. Kim, C.S.; Jeong, S.M.; Koo, W.H.; Baik, H.K.; Lee, S.-J.; Song, K.M. Synthesis of B–C–N nanotubes by means of gas arc discharge with a rotating anode. *Mater. Lett.* **2004**, *58*, 2878–2881. [[CrossRef](#)]
16. Schedin, F.; Geim, A.K.; Morozov, S.V.; Hill, E.W.; Blake, P.; Katsnelson, M.I.; Novoselov, K.S. Detection of individual gas molecules adsorbed on graphene. *Nat. Mater.* **2007**, *6*, 652–655. [[CrossRef](#)]
17. Di, C.-A.; Wei, D.; Yu, G.; Liu, Y.; Guo, Y.; Zhu, D. Patterned Graphene as Source/Drain Electrodes for Bottom-Contact Organic Field-Effect Transistors. *Adv. Mater.* **2008**, *20*, 3289–3293. [[CrossRef](#)]
18. Talla, J.A. Band gap tuning of defective silicon carbide nanotubes under external electric field: Density functional theory. *Phys. Lett. A* **2019**, *383*, 2076–2081. [[CrossRef](#)]
19. Akhtarianfar, S.F.; Shojaei, S. Location-dependent Stone-Wales defect in C/BN heteronanotube: A density functional theory approach. *Phys. E Low-Dimens. Syst. Nanostruct.* **2019**, *113*, 103–108. [[CrossRef](#)]
20. Guo, H.; Zhang, W.; Lu, N.; Zhuo, Z.; Zeng, X.C.; Wu, X.; Yang, J. CO₂ Capture on h-BN Sheet with High Selectivity Controlled by External Electric Field. *J. Phys. Chem. C* **2015**, *119*, 6912–6917. [[CrossRef](#)]
21. Lee, Y.; Kwon, D.-G.; Kim, G.; Kwon, Y.-K. Ab initio study of aspirin adsorption on single-walled carbon and carbon nitride nanotubes. *Phys. Chem. Chem. Phys.* **2017**, *19*, 8076–8081. [[CrossRef](#)] [[PubMed](#)]
22. Ouyang, J. Application of nanomaterials in two-terminal resistive-switching memory devices. *Nano Rev.* **2010**, *1*, 5118. [[CrossRef](#)] [[PubMed](#)]
23. Talla, J.A.; Salman, S.A. Electronic Structure Tuning and Band Gap Engineering of Carbon Nanotubes: Density Functional Theory. *Nanosci. Nanotechnol. Lett.* **2015**, *7*, 381–386. [[CrossRef](#)]
24. Salman, S.A.; Talla, J.A.; Al-Othoum, M.A. Uniaxial tension/compression effects on the electrical properties of carbon nanotube bundles: A first-principles study. *Mater. Express* **2018**, *8*, 353–360. [[CrossRef](#)]
25. Monkhorst, H.J.; Pack, J.D. Special points for Brillouin-zone integrations. *Phys. Rev. B* **1976**, *13*, 5188. [[CrossRef](#)]
26. Li, Y.; Zhou, Z.; Golberg, D.; Bando, Y.; Schleyer, A.P.V.R.; Chen, Z. Stone–Wales Defects in Single-Walled Boron Nitride Nanotubes: Formation Energies, Electronic Structures, and Reactivity. *J. Phys. Chem. C* **2008**, *112*, 1365–1370. [[CrossRef](#)]
27. Fan, Y.; Zhao, M.; He, T.; Wang, Z.; Zhang, X.; Xi, Z.; Zhang, H.; Hou, K.; Liu, X.; Xia, Y. Electronic properties of BN/C nanotube heterostructures. *J. Appl. Phys.* **2010**, *107*, 094304. [[CrossRef](#)]
28. Ivanovskaya, V.V.; Zobelli, A.; Stéphan, O.; Briddon, P.R.; Colliex, C. BN Domains Included into Carbon Nanotubes: Role of Interface. *J. Phys. Chem. C* **2009**, *113*, 16603–16609. [[CrossRef](#)]
29. Huang, C.; Chen, C.; Zhang, M.; Lin, L.; Ye, X.; Lin, S.; Antonietti, M.; Wang, X. Carbon-doped BN nanosheets for metal-free photoredox catalysis. *Nat. Commun.* **2015**, *6*, 7698. [[CrossRef](#)]
30. Salman, S.; Rekik, N.; Abuzir, A.; Suleiman, J. Electronic properties tuning of defective heterostructured CBN nanotubes by uniaxial pressure: A density functional study. *Appl. Phys. A* **2021**, *127*, 914. [[CrossRef](#)]
31. Serhan, M.; Abusini, M.; Almahmoud, E.; Omari, R.; Al-Khaza'Leh, K.; Abu-Farsakh, H.; Ghozlan, A.; Talla, J. The electronic properties of different chiralities of defected boron nitride nanotubes: Theoretical study. *Comput. Condens. Matter* **2020**, *22*, e00439. [[CrossRef](#)]

32. Tien, L.-G.; Liaw, T.-M.; Li, F.-Y.; Lin, S.-H.; Lee, M.-H.; Clark, S. Density-Functional-Theory Calculation of Semiconducting Carbon Nanotubes under an External Electric Field. *J. Chin. Chem. Soc.* **2003**, *50*, 627–629. [[CrossRef](#)]
33. Luo, Y.-P.; Tien, L.-G.; Tsai, C.-H.; Lee, M.-H.; Li, F.-Y. Effect of vacancy defect on electrical properties of chiral single-walled carbon nanotube under external electrical field. *Chin. Phys. B* **2011**, *20*, 017302. [[CrossRef](#)]
34. Shtogun, Y.V.; Woods, L.M. Electronic Structure Modulations of Radially Deformed Single Wall Carbon Nanotubes under Transverse External Electric Fields. *J. Phys. Chem. C* **2009**, *113*, 4792–4796. [[CrossRef](#)]
35. Kan, B.; Ding, J.; Yuan, N.; Wang, J.; Chen, Z.; Chen, X. Transverse electric field-induced deformation of armchair single-walled carbon nanotube. *Nanoscale Res. Lett.* **2010**, *5*, 1144–1149. [[CrossRef](#)]
36. Al-Sharif, A.; Almahmoud, E.; Talla, J.; Al-Khaza'Leh, K.; Ghozlan, A.; Samara, Q. Influence of external electric field on electronic and magnetic properties of doped boron nitride monolayer: Theoretical study. *Comput. Condens. Matter* **2020**, *25*, e00513. [[CrossRef](#)]